Inorganic Chemistry

Article

pubs.acs.org/IC

Enhanced Near-Infrared to Visible Upconversion Nanoparticles of Ho^{3+}-Yb^{3+}-F^- Tri-Doped TiO_2 and Its Application in Dye-Sensitized Solar Cells with 37% Improvement in Power Conversion Efficiency

Jia Yu,[†] Yulin Yang,*[,†] Ruiqing Fan,*[,†] Danqing Liu,[†] Liguo Wei,[†] Shuo Chen,[†] Liang Li,[†] Bin Yang,[‡] and Wenwu Cao*[,‡,§]

[†]Department of Chemistry, Harbin Institute of Technology, Harbin 150001, China

[‡]Condensed Matter Science and Technology Institute, Harbin Institute of Technology, Harbin 150080, China

[§]Materials Research Institute, The Pennsylvania State University, University Park, Pennsylvania 16802, United States

Supporting Information

ABSTRACT: New near-infrared (NIR)-to-green upconversion nanoparticles of Ho^{3+}-Yb^{3+}-F^- tridoped TiO_2 (UC-F-TiO_2) were designed and fabricated via the hydrosol−hydrothermal method. Under 980 nm NIR excitation, UC-F-TiO_2 emit strong green upconversion fluorescence with three emission bands at 543, 644, and 751 nm and convert the NIR light *in situ* to the dye-sensitive visible light that could effectively reduce the distance between upconversion materials and sensitizers; thus, they minimize the loss of the converted light. Our results show that this UC-F-TiO_2 offers excellent opportunities for the other types of solar cells applications, such as organic solar cells, c-Si solar cells, multijunction solar cells, and so on. When integrating the UC-F-TiO_2 into dye-sensitized solar cells (DSSCs), superior total energy conversion efficiency was achieved. Under AM1.5G light, open-circuit voltage reached 0.77 ± 0.01 V, short-circuit current density reached 21.00 ± 0.69 mA cm^{-2}, which resulted in an impressive overall energy conversion efficiency of 9.91 ± 0.30%, a 37% enhancement compared to DSSCs with pristine TiO_2 photoanode.

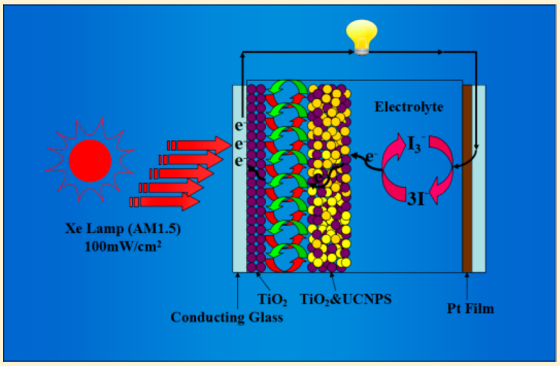

INTRODUCTION

Upconversion materials have the ability to convert lower energy (near-infrared (NIR) or infrared (IR)) radiation into high-energy radiation (ultraviolet or visible) via multiphoton absorption and energy transfer (ET) processes,[1] which are promising for applications in optical bioimaging,[2,3] biodetection,[4,5] clinical diagnosis,[6] three-dimensional display technologies,[7] photocatalysis,[8] as well as solar cells.[9−13]

Dye-sensitized solar cells (DSSCs) have gained increasing attention in the renewable energy research for relatively low production cost, more environmental-friendly manufacture process, and high efficiency.[14,15] Since Grätzel's group reset a new record of 10% in 1993, the highest conversion efficiency of DSSCs has plateaued over the past two decades,[16−21] and the spectral response of those devices in the NIR region is still limited.[22−24] Generally, the conversion efficiency of DSSCs can be influenced by many factors, such as light harvesting efficiency, electron injection efficiency, as well as the rate of undesirable charge recombination.[24] At present, the most commonly used sensitizers have an absorption threshold below 800 nm, so the development of efficient panchromatic sensitizers (400−1200 nm) seems to be a strategy to extend the energy conversion spectra, which can utilize NIR light to improve the light harvesting capability.[24,25] But poor electron injection efficiency and competing charge recombination of the panchromatic sensitizers hampered their development.[24,26] Upconversion materials are an alternative candidate to utilize the NIR light and thereby increase the light harvesting as well as the conversion efficiency of DSSCs. In the past few years, β-$NaYF_4$ had received intensive attention and had been proved to be one of the most effective host lattices for lanthanide ions to enhance their upconversion luminescence.[10,11,13,27] However, the relative separation distance between the sensitizer and the upconversion materials limited the energy transfer efficiency.[26]

In this work, we fabricated Ho^{3+}-Yb^{3+}-F^- tridoped TiO_2 (UC-F-TiO_2), which can be excited in the NIR spectral region. Under the excitation of 980 nm NIR light, the UC-F-TiO_2 emitted strong green upconversion fluorescence. Compared with the undoped TiO_2, UC-F-TiO_2's beauty associates with the *in situ* upconversion process, enhanced light harvesting, effective photogenerated electron−hole pair separation, as well as elevated Femi level, which will offer great opportunities to the modified DSSCs. For example, it can convert the NIR light *in situ* to the dye-sensitive visible light, shorten the distance between the upconversion material and sensitizer so as to take

Received: May 4, 2014
Published: July 14, 2014

 © 2014 American Chemical Society dx.doi.org/10.1021/ic501041h | Inorg. Chem. 2014, 53, 8045−8053

full advantage of the upconverted light. When the UC-F-TiO_2 was incorporated into DSSCs, substantial improvement was found. An overall conversion efficiency of 10.00% was achieved when this UC-F-TiO_2 was introduced into the bilayer-structured photoanode, corresponding to 37% improvement compared with the 7.19 ± 0.13% efficiency for DSSCs with a pristine TiO_2 photoanode.

EXPERIMENTAL SECTION

Synthesis of UC-F-TiO_2 Nanoparticles. The rare earth oxides [Ho_2O_3 and Yb_2O_3] were dissolved by using HNO_3 at the elevated temperature. The excess HNO_3 was evaporated, and then 2 mL of deionized water was added for use. We fabricated the UC-F-TiO_2 through hydrosol−hydrothermal method. HNO_3 (0.5 mL) and a certain amount of HF were added to 60 mL of deionized water; when the solution had been mixed well, 4.8 mL of tetrabutyl titanate were added over the course of 20−30 min while keeping intense stirring in the solution. This gives a flaky white precipitate. The solution was heated with vigorous stirring to nearly 100 °C (more like 90−95 °C) for 2 h, and the white precipitate seems to redissolve, giving a transparent light-blue hydrosol. Rare earth nitrate [$Ho(NO_3)_3$ and $Yb(NO_3)_3$] solution was then added slowly into the hydrosol under high-intense stirring. After the solution was stirred for 30 min, the obtained product was transferred into a Teflon-lined stainless steel autoclave and hydrothermally treated at 200 °C for 24 h. The obtained white precipitates were filtrated, washed by deionized water and absolute ethanol several times, dried at 100 °C for 6 h, and then calcined at 500 °C for 2 h; UC-F-TiO_2 nanoparticles were obtained.

Preparation and $TiCl_4$ Post-Treatment of Photoanode. Photoanode film was prepared by screen print method. Different composition ratio of UC-F-TiO_2 and commercial TiO_2 pastes were prepared for screen printing. Reference TiO_2 paste was prepared for comparison and the device fabrication had been reported previously in the literature.[28] The prepared photoanodes were soaked in dye N719 for 24 h (UV−vis absorption spectrum of N719 in ethanol solution and chemical structure are shown in Supporting Information, Figure S1). The post-treatment with $TiCl_4$ was applied to the sintered photoanodes, through immersing in 0.04 mol/L $TiCl_4$ solution at 75 ± 1 °C for 30 min, dried at 100 °C for 1h, and then sintered at 500 °C for 15 min.

Characterization. The morphology and structure of UC-F-TiO_2 were examined by scanning electron microscopy (SEM) (Rili SU 8000), transmission electron microscopy (TEM) (Tecnia G20, USA), and X-ray powder diffraction (XRPD) (Shimadzu XRD-6000). X-ray photoelectron spectra (XPS) were recorded by ESCALAB-250 spectrometer (Thermo, America). Ultraviolet visible near-infrared (UV−vis−NIR) absorption spectra were measured by UV-3600 spectrophotometer (SHIMADZU, JAPAN). Fourier transform infrared (FT-IR) spectra were taken by a Nicolet Avatar-360 infrared spectrometer. Fluorescence spectra were characterized by fluorescence spectrometer (Edinburgh FLS 920). Surface photovoltage spectroscopy (SPS) instrument was self-assembled with a 500 W xenon lamp, a lock-in amplifier (SR830-DSP), and a light chopper (SR540). Photocurrent−voltage characteristic curves and electrochemical impedance spectra (EIS) of the devices were carried out by electrochemical workstation (CHI660D, China). Incident photon-to-electron conversion efficiency (IPCE) spectra were measured using Newport IPCE measurement system. The controlled intensity modulated photospectroscopy was measured by photoelectrochemical workstation (Zahner CIMPS, Germany).

RESULTS AND DISCUSSION

Transmission electron microscopy (TEM) image shows that the morphology of UC-F-TiO_2 is predominantly random (Figure 1A). Compared with the pure TiO_2 (see Supporting Information, Figure S2A), there is no distinguishable difference in terms of morphology, indicating that fluorine ions have no influence on the morphology in our fabrication process. The

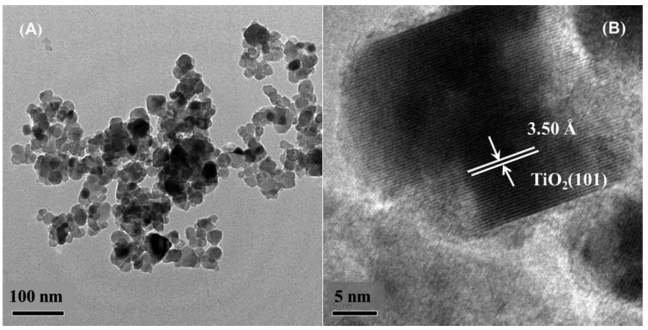

Figure 1. (A) TEM image of Ho^{3+}-Yb^{3+}-F^- tridoped TiO_2 (UC-F-TiO_2) and (B) high-resolution TEM image of one single UC-F-TiO_2.

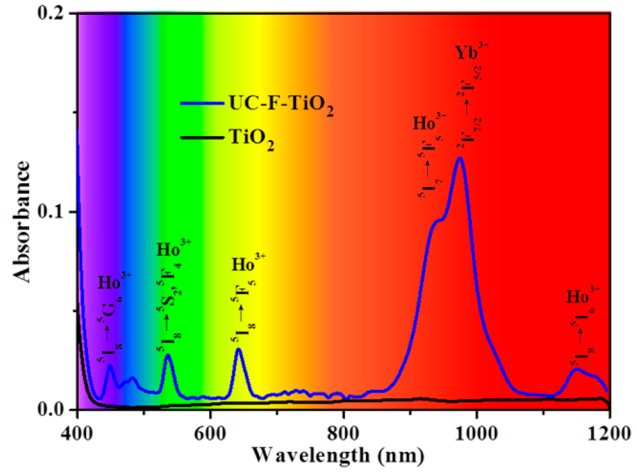

Figure 2. Partial magnified UV−vis−NIR absorption spectra for TiO_2 and UC-F-TiO_2.

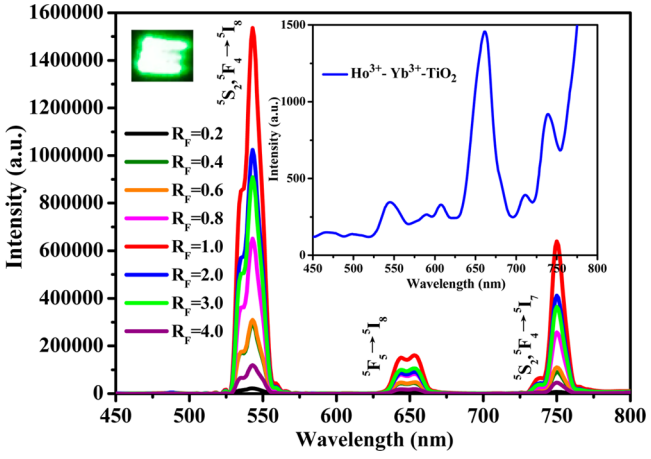

Figure 3. Upconversion fluorescence spectra of Ho^{3+}-Yb^{3+}-TiO_2 (inset) and UC-F-TiO_2 with different R_F values, excited under the same test condition by 980 nm NIR.

average sizes of the UC-F-TiO_2 are estimated to be 12−35 nm (see Supporting Information, Figure S2B). And the high-resolution TEM (Figure 1B) shows clear lattice fringes with spacing of ∼3.50 Å, which is consistent with the *d* spacing of (101) facets in TiO_2 (JCPDS 21−1272).

Supporting Information, Figure S3 gives the XPS spectra of the UC-F-TiO_2. The elemental composition of the UC-F-TiO_2 is revealed in Supporting Information, Figure S3A. The inset of Supporting Information, Figure S3A is the XPS spectrum for

dx.doi.org/10.1021/ic501041h | Inorg. Chem. 2014, 53, 8045−8053

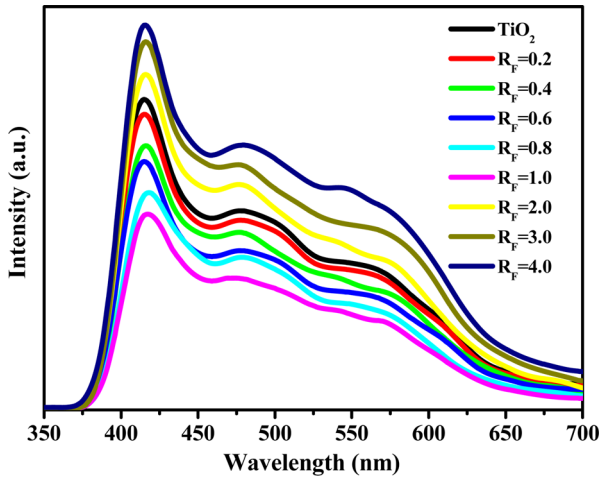

Figure 4. Fluorescence spectra curves of TiO_2 and UC-F-TiO_2, excited at 285 nm UV light.

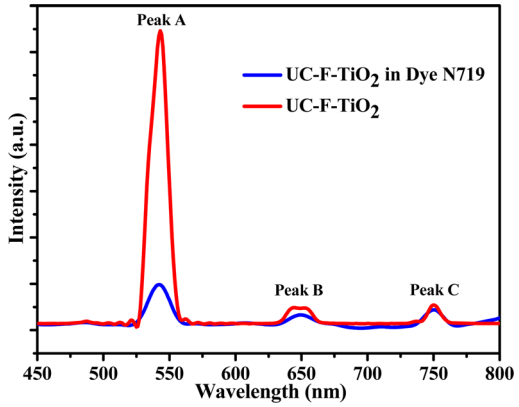

Figure 5. Upconversion fluorescence spectra of the UC-F-TiO_2 and N719 dye-sensitized UC-F-TiO_2 with 980 nm NIR excitation.

Scheme 1. Diagram of the Bilayer Structure DSSCs Device Consisting of a Bottom Layer of TiO_2 and a Top Layer of UC-F-TiO_2 Mixed with TiO_2

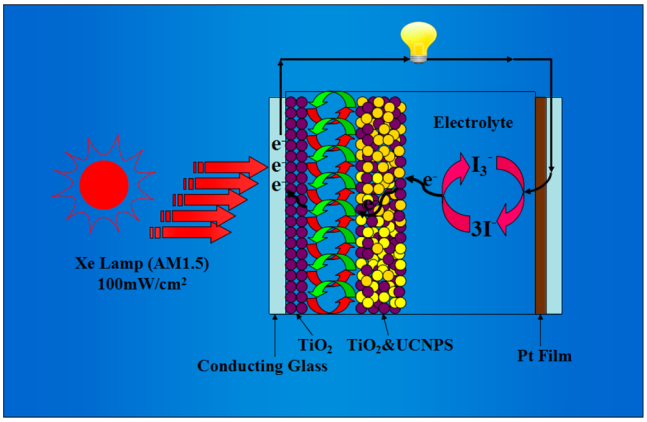

Ho 4d. The quite low spectral intensity of Ho^{3+} in UC-F-TiO_2 is due to two reasons: first, the concentration of Ho^{3+} is small, and second, the sensitivity factor of Ho^{3+} is smaller than that of Yb^{3+}; the binding energy of Ho^{3+} is very close to Yb^{3+} ion. The F 1s region consists of two peaks (Supporting Information, Figure S3B): one peak located at 684.9 eV should derive from the surface fluorine ions, and the other centered at 686.8 eV

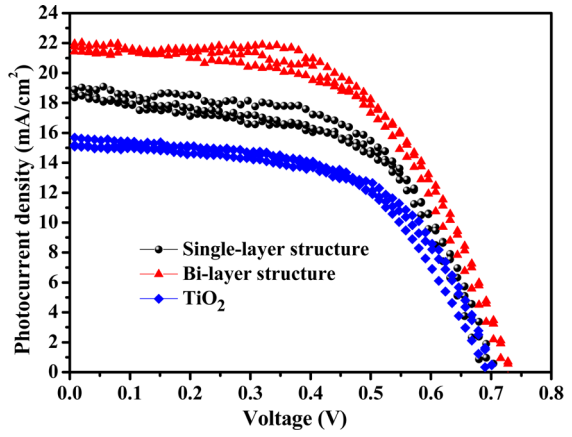

Figure 6. Photocurrent−voltage curves of DSSCs with different structure photoanodes under AM1.5G light, and the film thickness are the same.

should be ascribed to the fluorine ions doped in TiO_2.[29−31] In addition, the atomic contents of UC-F-TiO_2 are listed in Supporting Information, Table S1.

From the XRD patterns of UC-F-TiO_2 in Supporting Information, Figure S4, we can see that the diffraction lines are all assignable to anatase TiO_2 (JCPDS 21−1272) and YbF_3 (JCPDS 49−1805). Yb^{3+} ions probably react with the surface fluorine ions and form into YbF_3, so we did not find its interlayer spacing.

Figure 2 shows the magnified UV−vis−NIR absorption spectra of TiO_2 and UC-F-TiO_2 (the original UV−vis−NIR absorption spectra is in Supporting Information, Figure S5), which indicates that UC-F-TiO_2 expands the TiO_2 absorption in the range of visible light and extends it to the IR region. There are six characteristic absorption peaks at the wavelengths around 453, 543, 644, 939, 1154, and 976 nm, corresponding to the transitions $^5I_8 \rightarrow {}^5G_6$, $^5I_8 \rightarrow ({}^5S_2, {}^5F_4)$, $^5I_8 \rightarrow {}^5F_5$, $^5I_7 \rightarrow {}^5F_5$, and $^5I_8 \rightarrow {}^5I_6$ for Ho^{3+} ions and $^2F_{7/2} \rightarrow {}^2F_{5/2}$ for Yb^{3+} ions.[32]

Upconversion fluorescence was excited by a 980 nm laser. As shown in Figure 3, fluorine ions can enhance the upconversion fluorescence intensity of UC-F-TiO_2, and therefore UC-F-TiO_2 exhibits a stronger peak around 543 nm and two relatively weaker peaks, one of which is centered at 644 nm; the other is located at 751 nm. The dominant green emission centered at 543 nm is assigned to the transition from $({}^5S_2, {}^5F_4)$ levels to the $^5I_8$ ground state. The two weaker emissions observed in the red region centered at 644 and 751 nm are caused by the $^5F_5 \rightarrow {}^5I_8$ transition and the $({}^5S_2, {}^5F_4) \rightarrow {}^5I_7$ transition, respectively. Supporting Information, Figure S6 shows the FT-IR spectra of the UC-F-TiO_2, including Ho^{3+},Yb^{3+}-TiO_2, used here as a reference. As we can see, fluorine ions weaken the OH absorption band (around 3400 cm^{-1}), which indicates that the enhanced upconversion fluorescence intensity should be ascribed to reduced OH groups. It is well-known that OH groups can increase the nonradiative relaxation rate for its high vibration frequency and lead to poor upconversion efficiency.[33,34] The FTIR spectra of the vibration of Ti−O stretching mode is in the range of 400−800 cm^{-1}.[35,36] After adding fluorine ions, the broad peak belongs to this blue-shifted region, which means the phonon energy of host decreased. Host materials with low phonon energy can lower the nonradiative relaxation probability and enhance the luminescence efficiency. However, when the mole ratio of F^- and Ti^{4+} (R_F) value is over 1.0, new defect sites may be introduced,

dx.doi.org/10.1021/ic501041h | Inorg. Chem. 2014, 53, 8045−8053

Table 1. Photovoltaic Parameters of a Series of DSSCs Based on UC-F-TiO_2

UC-F-TiO_2/TiO_2	Jsc, mA cm^{-2}	Voc, V	FF	η, %	amount of dye, mol $cm^{-2} \times 10^{-8}$
1:0	8.17 ± 0.30	0.77 ± 0.01	0.61 ± 0.02	3.82 ± 0.12	5.40 ± 0.01
4:6	18.44 ± 0.76	0.74 ± 0.01	0.56 ± 0.02	7.65 ± 0.30	7.80 ± 0.01
3:7	21.60 ± 0.62	0.73 ± 0.01	0.57 ± 0.01	8.93 ± 0.06	8.20 ± 0.01
2:8	18.00 ± 0.55	0.72 ± 0.01	0.58 ± 0.01	7.49 ± 0.09	8.20 ± 0.01
0:1	15.59 ± 0.38	0.71 ± 0.01	0.57 ± 0.01	6.34 ± 0.05	9.60 ± 0.01

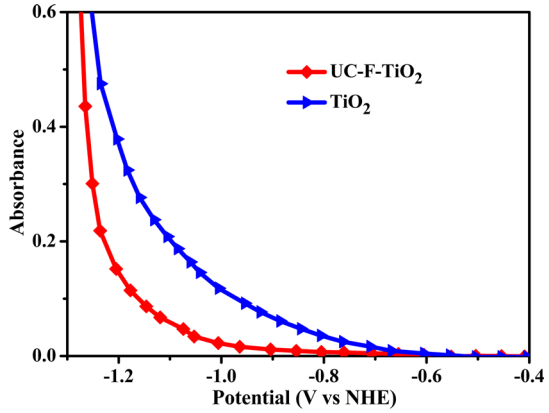

Figure 7. Optical absorbance of the TiO_2 and UC-F-TiO_2 film electrode immersed in 0.1 M $LiClO_4$ at 780 nm, under different potentials.

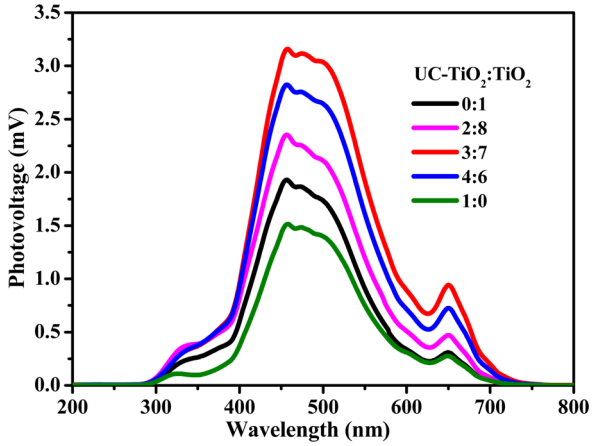

Figure 8. Effect of UC-F-TiO_2 nanoparticles (wt %) on the surface photovoltage spectra of DSSCs.

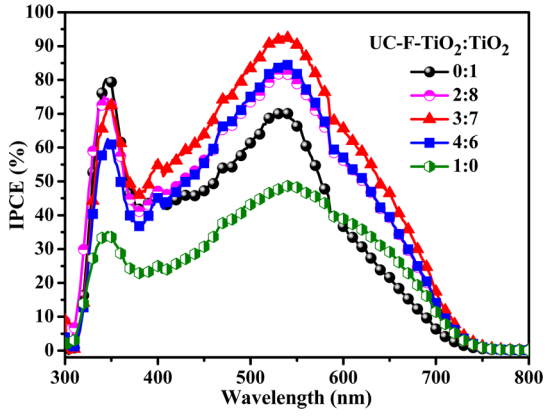

Figure 9. Effect of UC-F-TiO_2 nanoparticles (wt %) on IPCE spectra of DSSCs.

which will increase the possibility of nonradiative relaxations, consequently leading to poor luminescence efficiency.

Fluorescence spectra technique has been widely used in solid semiconductors to help understand surface transport process of photogenerated electrons and holes. Figure 4 shows the fluorescence spectra of TiO_2 and UC-F-TiO_2, under the excitation of 285 nm UV light. Although the emission spectra shapes are similar, the emission intensity between R_F = 0 and R_F = 1.0 decreases, which indicates that fluorine ions can retard the radiative recombination process of charge carriers in TiO_2 and thus improve the injection efficiency of photon-generated electrons. However, samples with excessive fluorine ions (R_F = 2.0, 3.0, 4.0) exhibit obvious increases in the emission intensity. This is probably because some new defects or recombination centers are introduced and cause more photogenerated electrons recombined with holes instead of injecting immediately.[29] Our fluorescence spectra measurement results confirmed that the lower the intensity of fluorescence spectra was, the stronger the upconversion fluorescence that was emitted, and this result was in good agreement with the above discussion. In the next section, our discussion will based on the UC-F-TiO_2 with R_F = 1.0.

Aiming to understand the mechanism, the dependence of green and red upconversion emissions of UC-F-TiO_2 on the excitation power was analyzed.[1,26] As we can see from Supporting Information, Figure S7, slope values of 2.33, 2.33, and 2.11 are observed for the upconversion emissions at 543, 644, and 751 nm, which indicate that a two-photon process is involved in the fluorescence generation. Supporting Information, Figure S8 is the CIE chromaticity coordinates of the spectra; the spectral power is multiplied by each of the three color matching functions, but only two chromaticity coordinates (x, y) are calculated.[37] The CIE coordinate is (0.26, 0.30) as shown in Supporting Information, Figure S8.

To unequivocally verify the energy transfer path between the UC-F-TiO_2 and the sensitizer N719 dye, upconversion fluorescence spectra of the UC-F-TiO_2 and N719 dye-sensitized UC-F-TiO_2 were obtained and shown in Figure 5. There are three upconversion emission bands with peaks at ~543 nm (peak A), ~644 nm (peak B), and ~751 nm (peak C). As we can see from Figure 5, the emission intensities of those three peaks decreased after dye sensitizing. After adding N719 dye, peak A decreased by ~7.6 times, peak B decreased by ~1.7 times, while peak C decreased by ~1.2 times. This result proves that, during the energy-transfer process, peak A is crucial for enhancing the energy transfer, and it is much more efficient than the other two peaks. This also confirmed that the green emission at ~543 nm generated by the UC-F-TiO_2 nanoparticles *in situ* can be effectively reutilized by the dye-sensitizer. The upper absorption limit of N719 is about 700 nm, thus the decrease of peak B and peak C are lower.

We applied the UC-F-TiO_2 in dye-sensitized solar cells, assembled it into a bilayer-structured photoanode to improve the capability of light harvesting so as to achieve better DSSCs

dx.doi.org/10.1021/ic501041h | Inorg. Chem. 2014, 53, 8045−8053

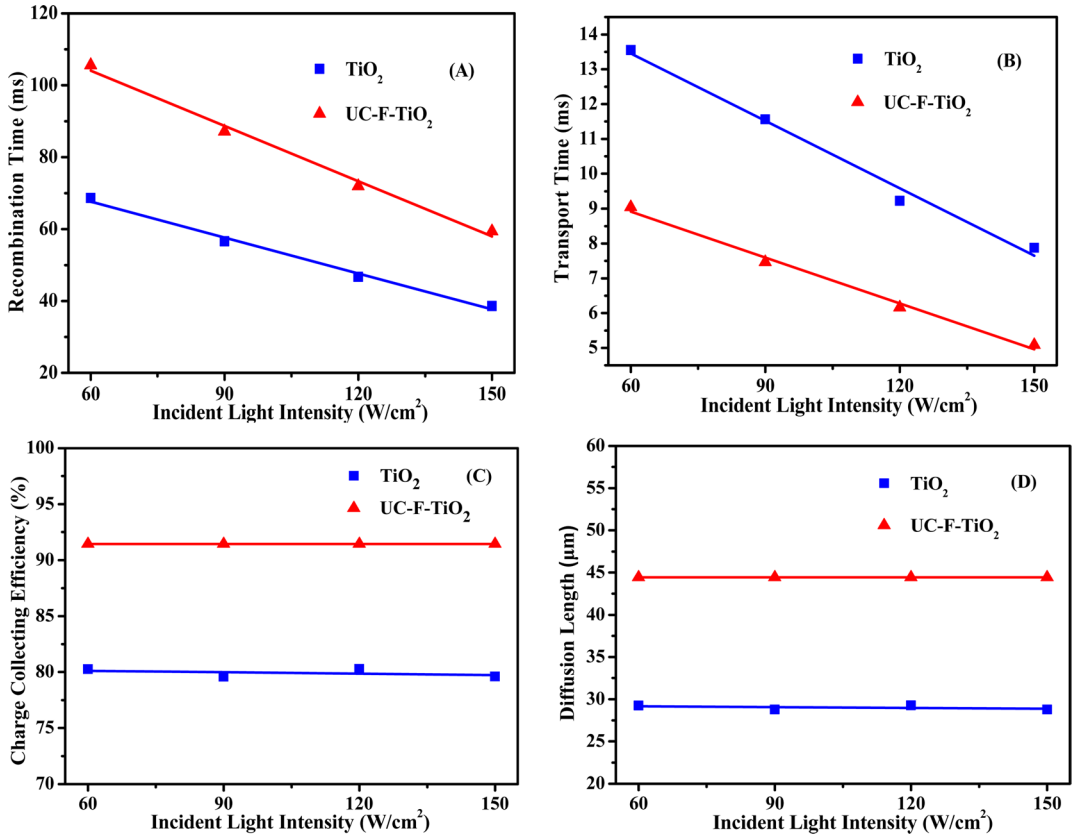

Figure 10. (A) Intensity-modulated photovoltage spectra. (B) Intensity-modulated photocurrent spectra. (C) Charge collection efficiency. (D) Electron diffusion length of TiO_2 photoanode and bilayer-structure of UC-F-TiO_2 photoanode.

efficiency. The photoanode thickness of compared TiO_2, single layer-structured and the bilayer-structured UC-F-TiO_2 are the same (12 μm). Scheme 1 presents the configuration of our DSSCs device, which consists of a bilayer-structured photoanode with TiO_2 as bottom layer (4 μm) and UC-F-TiO_2 mixed with TiO_2 as top layer (8 μm). Compared with UC-F-TiO_2, TiO_2 with average primary particle size of 21 ± 5 nm has better adherence with the FTO glass. Thus, TiO_2 as bottom layer is beneficial for electron transport. The top layer consisting of UC-F-TiO_2 can convert the NIR light into visible light *in situ*, shortening the distance between the UC material and sensitizer so as to improve the solar light harvesting. As we can see from Figure 6, bilayer-structured photoanode-assembled DSSCs have the best performance. To confirm the overall efficiency of DSSCs has been improved by the upconversion nanoparticles, we conducted the following experiments. Under the same experimental conditions, we chose a spectral filter of 645 nm to block the main absorbed light of N719 under AM1.5G light. As can be seen in Supporting Information, Figure S9, the short-circuit current density (J_{SC}) of UC-F-TiO_2 formed by DSSCs is 7.32 mA cm^{-2}, which was 1.14 times higher than that of the device with TiO_2 (J_{SC} = 6.41 mA cm^{-2}). This apparent enhancement of the photocurrent suggests that the presence of the UC-F-TiO_2 can transform the NIR light into visible light, which can be used by N719.

Photovoltaic parameters of a series of DSSCs based on UC-F-TiO_2 are listed in Table 1. And this result is based on the average of five photoanodes for each photoanode material (for details, see Supporting Information, Table S2). As the wt % of UC-F-TiO_2 is increased, the open-circuit voltage V_{OC} gets higher, the amount of dye-loading gets smaller, and J_{sc} rises first and then descends. The DSSCs device gains a maximum conversion efficiency of 8.93 ± 0.06%, while the top layer content of UC-F-TiO_2 is 30 wt %. Compared with the reference TiO_2 DSSCs, the amount of dye-loading in UC-F-TiO_2-composed DSSCs is lower. This is related to the size of UC-F-TiO_2 nanoparticles, which is heterogeneous comparing with TiO_2. When the top layer wt % of UC-F-TiO_2 is less than 30 wt %, the increased J_{sc} should be attributed to the upconversion effect. But, when the top layer wt % is over 30, more grains, phases, as well as interfaces will be introduced. These defects will diminish the photocurrent by capturing photogenerated electrons and, thereby, hinder the electron transport.[38−40]

The flat band potential (V_{fb}) is an effective way to locate the energetic edge position of the conduction and the valence band.[41] There are two common methods to assess the value of V_{fb}, namely, spectroelectrochemical measurements[42] and Mott−Schottky analyses of the impedance spectra.[43,44] In our experiment, we got the value of V_{fb} by spectroelectrochemical method, which was proposed by Michael Grätzel. The intraband transitions and free carrier absorption could cause an obvious optical absorption at 780 nm; thus, the absorbance in this wavelength indicates the electron density of the conduction band.[41] We changed the applied potential from 0.2 to −1.3 V and recorded the corresponding absorbance at 780 nm. As we can see in Figure 7, the flat band of TiO_2 shifts from −0.6 to −0.75 V, which implies the Fermi level of UC-F-TiO_2 is higher than that of TiO_2. This is the reason why the V_{OC} increases with UC-F-TiO_2 amount in the top layer of the DSSCs.

dx.doi.org/10.1021/ic501041h | *Inorg. Chem.* 2014, 53, 8045−8053

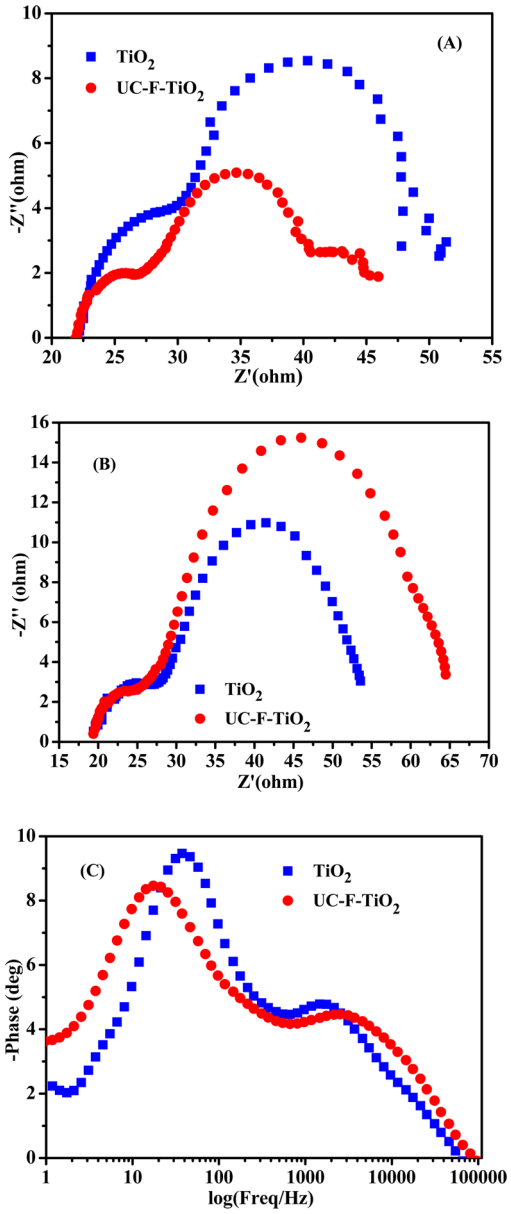

Figure 11. (A) Nyquist plots of DSSCs with bilayer structure UC-F-TiO_2 and TiO_2 photoanodes under AM1.5G light. (B) Nyquist plots of DSSCs in the dark. (C) Bode-phase plots of DSSCs under AM1.5G light.

Table 2. Resistances Simulated Based on Equivalent Circuit

	under AM1.5G light			in the dark		
type	R_s, Ω	R_1, Ω	R_2, Ω	R_s, Ω	R_1, Ω	R_2, Ω
TiO_2	53.44	9.64	17.03	20.03	4.00	14.15
UC-F-TiO_2	21.61	8.41	9.60	23.10	5.62	18.48

Figure 8 reveals the effect of UC-F-TiO_2 nanoparticles (wt %) on the surface photovoltage spectra of DSSCs. The SPS response of UC-F-TiO_2 (30 wt %) is very strong, indicating that the sample has high separation probability of photoexcited carriers. This improvement may be attributed to two reasons: (1) the upconversion effect, the upconversion emission bands centered at ~543 nm and ~644 nm, which lead to an increased response in visible light region, and (2) the effective separation of the photon-generated electrons, which affects photoelectric

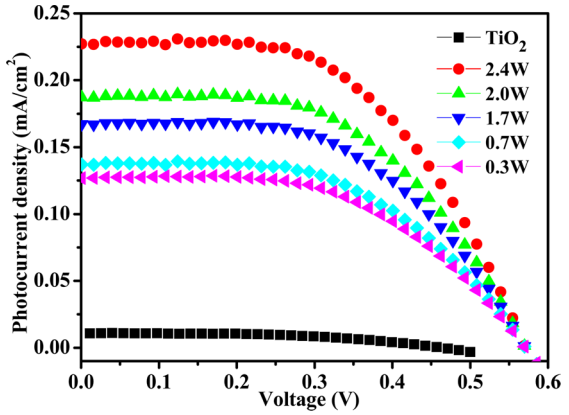

Figure 12. *I*–*V* curves of DSSCs under 980 nm laser light with different power supply.

conversion capability.[45,46] It is known that surface photovoltage will be reduced by high recombination of photon-generated electrons. However, the SPS response decreases inversely if the UC-F-TiO_2 content is too much. This can be caused by several factors, such as the efficiency of electron transport, the amount of dye-loading, and so on.

Figure 9 shows the typical curves of IPCE in the 400–800 nm wavelength range. It indicates that when the content of UC-F-TiO_2 is less than 30 wt %, the IPCE increases with the increased wt % of UC-F-TiO_2, which is caused by the upconversion effect of UC-F-TiO_2. However, when the wt % of UC-F-TiO_2 over 30, the IPCE value decreases, which can be attributed to the poor dye-loading.

Intensity-modulated photovoltage spectroscopy (IMVS) and photocurrent spectroscopy (IMPS) are two conventional methods to investigate the process of electron transfer and recombination in DSSCs. Figure 10A,B shows the IMVS response and the IMPS response of TiO_2 photoanode and the UC-F-TiO_2 photoanode (30 wt %). From the following eqs 1 to 4, we can estimate the values of electron recombination time (τ_n), electron transport time (τ_d), charge collection efficiency (η_{cc}), and electron diffusion length (L_n).[47]

$$\tau_n = 1/2\pi f_n \quad (1)$$

$$\tau_d = 1/2\pi f_d \quad (2)$$

$$\eta_{cc} = 1 - \tau_d/\tau_n \quad (3)$$

$$L_n = (L^2\tau_n/\tau_d)^{1/2} \quad (4)$$

Here, f_n and f_d are the minimum frequencies of the IMVS and IMPS curves, respectively; L is the thickness of photoanode film.

From Figure 10A,B, the UC-F-TiO_2 photoanode has a longer electron recombination time and a faster transport rate compared with TiO_2 photoanode. A high η can result from a higher η_{cc} and a longer L_n. The UC-F-TiO_2 photoanode has a better charge collection efficiency η_{cc} than that of the TiO_2 photoanode, because the bottom layer TiO_2 improves the adhesion of the bilayer UC-F-TiO_2 photoanode. And UC-F-TiO_2 mixed with TiO_2 as top layer, in which the fluorine ions retard the radiative recombination process of charge carriers and the elevated Fermi level, helps reduce the resistance of electrons transport. Thus, the DSSCs with UC-F-TiO_2 photoanodes achieve remarkably increased η_{cc} (Figure 10C).

dx.doi.org/10.1021/ic501041h | Inorg. Chem. 2014, 53, 8045–8053

Table 3. Photovoltaic Characteristics of DSSCs with Different Photoanodes

type[a]	Jsc (mA cm^{-2})	Voc (V)	FF	η (%)
TiO_2	16.80 ± 0.62	0.72 ± 0.02	0.60 ± 0.01	7.19 ± 0.13
UC-F-TiO_2	21.00 ± 0.69	0.77 ± 0.01	0.62 ± 0.01	9.91 ± 0.30

[a]TiO_2 and UC-F-TiO_2 photoanodes are post-treated with $TiCl_4$ solution, and these results are based on the average of five photoanodes for each photoanode material (for details, see Supporting Information, Table S3).

Scheme 2. Energy Transfer Mechanisms in the Upconversion Material UC-F-TiO_2

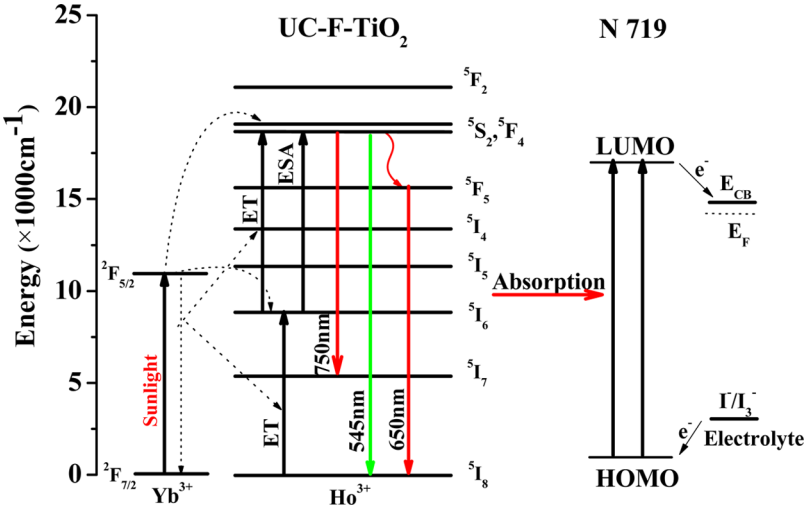

From the values of τ_n and τ_d, we can assess the electron diffusion length. Our experimental results in Figure 10D indicate that the UC-F-TiO_2 photoanode has a longer diffusion length compared with that of TiO_2 photoanode.

Figure 11A,B shows the Nyquist plot of the DSSCs based on TiO_2 and UC-F-TiO_2 photoanodes under illumination and in the dark. Supporting Information, Figure S10 shows the simulated equivalent circuit via ZSimpWin software: $R_s(C_1(R_1O_1))(R_2Q_2)$. R_s is the series resistance, R_1 is the charge transfer resistance of the Pt electrode, and R_2 is the transport or recombination resistance of the photoelectrode.[48] The simulated resistances are listed in Table 2. We changed the Pt electrode before assembling every new DSSC, so the R_1 values are different; under the 1.5G light, R_2 reduces from 17.03 to 9.60 Ω, which suggests that electrons can transport faster in DSSCs with UC-F-TiO_2 photoelectrode. In the dark, the value of R_2 represents the recombination resistance between the injected electron and the redox electrolyte (I_3^-). As we can see, the R_2 value of UC-F-TiO_2 composed DSSCs (18.48 Ω) is higher than that of TiO_2-composed DSSCs (14.15 Ω). Thus, the recombination process between the injected electron and the redox electrolyte is better hindered in the UC-F-TiO_2 photoelectron-based DSSCs.

The electron lifetime (Γ_{eff}) could be calculated from the midfrequency (f_{max}),

$$\Gamma_{eff} = 1/2\Pi f_{max} \quad (5)$$

where f_{max} is the peak frequency in the midfrequency range.[49] In Figure 11C, the TiO_2 photoanode's f_{max} value is higher than that of the UC-F-TiO_2 bilayer photoanode, and thus the value of Γ_{eff} for UC-F-TiO_2 bilayer photoanode is higher than that of TiO_2 photoanode. An increment in the Γ_{eff} value indicates, in the UC-F-TiO_2 photoelectron-based DSSCs, the probability of photoinjected electrons reacted with I_3^- ions is reduced.

To confirm the fact that the UC-F-TiO_2 nanoparticles-composed DSSCs can utilize the NIR light and generate photocurrents, we measured the $I-V$ response of the DSSCs with UC-F-TiO_2 and TiO_2 photoanodes under 980 nm light. As can be seen in Figure 12, little photocurrent is produced in the TiO_2 photoanode-composed DSSCs, and the photocurrent does not change with the laser power supply. However, the J_{SC} of UC-F-TiO_2 increases with the laser power supply, and the V_{OC} stays still. Thus, this apparent increment of the photocurrent demonstrates that the presence of the UC-F-TiO_2 transforms the NIR light into visible light, which can be used by N719 and generate photocurrent.

Compared with the DSSCs with TiO_2 photoanode (see Table 3), DSSCs with UC-F-TiO_2 have higher J_{sc} and V_{OC} because of the following reasons: (1) The absorption process in the energy transfer mechanism between the UC-F-TiO_2 and N719 dye, in which the fluorescence emissions of the UC-F-TiO_2, particularly the converted green light, are efficiently absorbed by N719. (2) V_{OC} corresponds to the energy level difference between the electrons in the TiO_2 photoanode and the redox potential of the electrolyte. When Ho^{3+}, Yb^{3+}, and F^- ions are tridoped in TiO_2, the flat-band potential and the Fermi level of the TiO_2 photoanode are elevated; thus, the V_{OC} is increased. (3) UC-F-TiO_2 converts the NIR light to the dye-sensitive visible light *in situ*, and the shorter distance between the upconversion nanoparticles and the dye sensitizer can ensure an effective energy relay from UC-F-TiO_2 to N719. Hence, we can see that the UC-F-TiO_2-based DSSCs achieved impressive photocurrent density–voltage ($I-V$) characteristics with the V_{OC} = 0.77 ± 0.01 V, short-circuit current density (J_{SC}) = 21.00 ± 0.69 mA cm^{-2}, and the overall energy conversion efficiency (η) = 9.91 ± 0.30%. Scheme 2 outlines the energy transfer mechanisms in the upconversion material UC-F-TiO_2.[32,50]

dx.doi.org/10.1021/ic501041h | Inorg. Chem. 2014, 53, 8045−8053

CONCLUSIONS

In summary, NIR-to-green upconversion fluorescent nanoparticles of Ho^{3+}-Yb^{3+}-F^- tridoped TiO_2 (UC-F-TiO_2) were designed and fabricated as advanced upconversion materials for making more efficient DSSCs. The improved DSSCs conversion efficiency is as large as 37%, which is associated with closer attachment of the *in situ* upconversion process, enhanced light harvesting, and photogenerated electron−hole pair separation, as well as elevated Femi level. UC-F-TiO_2 with excellent *in situ* NIR-to-green upconversion ability helps dye-sensitized solar cells to utilize more NIR light and offers excellent opportunities for the other types of solar cell applications, such as organic solar cells, c-Si solar cells, multijunction solar cells, and so on.

Although dye-sensitized solar cells have many advantages compared to silicon-based solar cells, particularly in terms of more environmental-friendly manufacture processes, its energy conversion efficiency is still lagging. The NIR-to-green upconversion fluorescent nanoparticles of Ho^{3+}-Yb^{3+}-F^- tridoped TiO_2 combined with other improvements in structure design optimization and the new sensitizers, such as panchromatic sensitizer, will soon make dye-sensitized solar cells with higher conversion efficiencies.

ASSOCIATED CONTENT

Supporting Information

UV−vis absorption spectrum and chemical structure of N719; SEM image of TiO_2 and the size distribution of UC-F-TiO_2; XPS survey spectrum of UC-F-TiO_2 and the F 1s region; XPS measured the content of UC-F-TiO_2 products; XRD pattern of the as-prepared UC-F-TiO_2; UV−vis−NIR absorption spectra for TiO_2 and UC-F-TiO_2; FT-IR spectra of Ho^{3+}, Yb^{3+}-TiO_2, and UC-F-TiO_2; dependence of UC-F-TiO_2 fluorescence intensity on the excitation power from a 980 nm laser at 543, 644, and 751 nm; CIE coordinate of the upconversion emission from UC-F-TiO_2, upon 980 nm NIR excitation; *I*−*V* curves of DSSCs with a spectral filter of 645 nm under AM1.5G light; summary of photovoltaic parameters of a series of DSSCs based on UC-F-TiO_2; equivalent circuit obtained by using ZSimpWin software: $R_s(C_1(R_1O_1))(R_2Q_2)$; summary of the device performance of DSSCs based on TiO_2 and UC-F-TiO_2 with $TiCl_4$ post-treatment. This material is available free of charge via the Internet at http://pubs.acs.org.

AUTHOR INFORMATION

Corresponding Authors

*E-mail: ylyang@hit.edu.cn. Fax: +86 451 86413710. (Y.Y.)
*E-mail: fanruiqing@hit.edu.cn. (R.F.)
*E-mail: dzk@psu.edu. (W.C.)

Notes

The authors declare no competing financial interest.

ACKNOWLEDGMENTS

This work was supported by National Natural Science Foundation of China (Grant Nos. 21171044 and 21371040), the National Key Basic Research Program of China (973 Program, No. 2013CB632900), supported by the Fundamental Research Funds for the Central Universities (Grant No. HIT. IBRSEM. A. 201409), and Program for Innovation Research of Science in Harbin Institute of Technology (PIRS of HIT Nos. A201416 and B201414).

REFERENCES

(1) Zou, W. Q.; Visser, C.; Maduro, J. A.; Pshenichnikov, M. S.; Hummelen, J. C. *Nat. Photonics* **2012**, *6*, 560−564.
(2) Zhan, Q. Q.; Qian, J.; Liang, H. J.; Somesfalean, G.; Wang, D.; He, S. L.; Zhang, Z. G.; Engels, S. A. *ACS Nano* **2011**, *5*, 3744−3757.
(3) Zhou, J. J.; Shirahata, N.; Sun, H. T.; Ghosh, B.; Ogawara, M.; Teng, Y.; Zhou, S. H.; Chu, R. G. S.; Fujii, M.; Qiu, J. R. *J. Phys. Chem. Lett.* **2013**, *4*, 402−408.
(4) Chen, G. Y.; Shen, J.; Ohulchanskyy, T. Y.; Patel, N. J.; Kutikov, A.; Li, Z. P.; Song, J.; Pandey, R. K.; Agren, H.; Prasad, P. N.; Han, G. *ACS Nano* **2012**, *6*, 8280−8287.
(5) Liu, Y. S.; Zhou, S. Y.; Tu, D. T.; Chen, Z.; Huang, M. D.; Zhu, H. M.; Ma, E.; Chen, X. Y. *J. Am. Chem. Soc.* **2012**, *134*, 15083−15090.
(6) Yi, G. J.; Peng, Y. F.; Gao, Z. Q. *Chem. Mater.* **2011**, *23*, 2729−2734.
(7) Wang, W.; Huang, W. J.; Ni, Y. R.; Lu, C. H.; Tan, L. J.; Xu, Z. Z. *Appl. Surf. Sci.* **2013**, *282*, 832−837.
(8) Gibart, P.; Auzel, F.; Guillaume, J. C.; Zahraman, K. *J. Appl. Phys.* **1996**, *35*, 4401−4402.
(9) Shalav, A.; Richards, B. S.; Green, M. A. *Sol. Energy Mater. Sol. Cells* **2007**, *91*, 829−842.
(10) Liang, L. L.; Liu, Y. M.; Bu, C. H.; Guo, K. M.; Sun, W. W.; Huang, N.; Peng, T.; Sebo, B.; Pan, M. M.; Liu, W.; Guo, S. S.; Zhao, X. Z. *Adv. Mater.* **2013**, *25*, 2174−2180.
(11) De Wild, J.; Meijerink, A.; Rath, J. K.; van Sark, W. G. J. H. M.; Schropp, R. E. I. *Energy Environ. Sci.* **2011**, *4*, 4835−4848.
(12) Shan, G. B.; Demopoulos, G. P. *Adv. Mater.* **2010**, *22*, 4373−4377.
(13) Shan, G. B.; Assaaoudi, H.; Demopoulos, G. P. *ACS Appl. Mater. Interfaces* **2011**, *3*, 3239−3243.
(14) O'Regan, B.; Grätzel, M. *Nature* **1991**, *353*, 737−740.
(15) Grätzel, M. *Inorg. Chem.* **2005**, *44*, 6841−6851.
(16) Hua, Y.; Chang, S.; Huang, D. D.; Zhou, X.; Zhu, X. J.; Zhao, J. Z.; Chen, T.; Wong, W. Y.; Wong, W. K. *Chem. Mater.* **2013**, *25*, 2146−2153.
(17) Sun, Z. Q.; Kim, J. H.; Zhao, X.; Attard, D.; Dou, S. X. *Chem. Commun.* **2013**, *49*, 966−968.
(18) Lapides, A. M.; Ashford, D. L.; Hanson, K.; Torelli, D. A.; Templeton, J. L.; Meyer, T. J. *J. Am. Chem. Soc.* **2013**, *135*, 15450−15458.
(19) Das, P. P.; Agarkar, S. A.; Mukhopadhyay, S.; Manju, U.; Ogale, S. B.; Devi, P. S. *Inorg. Chem.* **2014**, *53*, 3961−3972.
(20) Nazeeruddin, M. K.; Rodicio, A. K.; Baker, R. H.; Müller, E.; Liska, P.; Vlachopoulos, N.; Grätzel, M. *J. Am. Chem. Soc.* **1993**, *115*, 6382−6390.
(21) Chen, S. G.; Chappel, S.; Diamant, Y.; Zaban, A. *Chem. Mater.* **2001**, *13*, 4629−4634.
(22) Yella, A.; Lee, H. W.; Tsao, H. N.; Yi, C. Y.; Chandiran, A. K.; Nazeeruddin, M. K.; Yeh, C. Y.; Zakeeruddin, S. M.; Grätzel, M. *Science* **2011**, *334*, 629−634.
(23) Burschka, J. L.; Pellet, N.; Moon, S. J.; Baker, R. H.; Gao, P.; Nazeeruddin, M. K.; Grätzel, M. *Nature* **2013**, *499*, 316−319.
(24) Ning, Z. J.; Fu, Y.; Tian, H. *Energy Environ. Sci.* **2010**, *3*, 1170−1181.
(25) Li, G. C.; Ray, L.; Glass, E. N.; Kovnir, K.; Khoroshutin, A.; Gorelsky, S. I.; Shatruk, M. *Inorg. Chem.* **2012**, *51*, 1614−1624.
(26) Yuan, C. Z.; Chen, G. Y.; Prasad, P. N.; Ohulchanskyy, T. Y.; Ning, Z. J.; Tian, H. N.; Sund, L. C.; Agren, H. *J. Mater. Chem.* **2012**, *22*, 16709−16713.
(27) Li, C. X.; Quan, Z. W.; Yang, J.; Yang, P. P.; Lin, J. *Inorg. Chem.* **2007**, *46*, 6329−6337.
(28) Yu, J.; Yang, Y. L.; Fan, R. Q.; Li, L.; Li, X. Y. *J. Phys. Chem. C* **2014**, *118*, 8795−8802.
(29) Yu, J. C.; Yu, J. G.; Ho, W. K.; Jiang, Z. T.; Zhang, L. Z. *Chem. Mater.* **2002**, *11*, 3808−3816.
(30) He, Z. L.; Que, W. Q.; Chen, J.; Yin, X. T.; He, Y. C.; Ren, J. B. *ACS Appl. Mater. Interfaces* **2012**, *4*, 6816−6826.
(31) Subramanian, V.; Wolf, E. E.; Kamat, P. V. *J. Am. Chem. Soc.* **2004**, *126*, 4943−4950.

(32) Huang, X. Y.; Han, S. Y.; Huang, W.; Liu, X. G. *Chem. Soc. Rev.* **2013**, *42*, 173−201.
(33) Bai, Y. F.; Wang, Y. X.; Peng, G. Y.; Yang, K.; Zhang, X. R.; Song, Y. L. *J. Alloys Compd.* **2009**, *478*, 676−678.
(34) Guo, H.; Dong, N.; Yin, M.; Zhang, W. P.; Lou, L. R.; Xia, S. D. *J. Phys. Chem. B* **2004**, *108*, 19205−19209.
(35) Jiang, Y. H.; Luo, Y. Y.; Zhang, F. M.; Guo, L. Q.; Ni, L. *Appl. Surf. Sci.* **2013**, *273*, 448−456.
(36) Peiro, A. M.; Peral, J.; Domingo, C.; Momenech, X.; Ayllon, J. A. *Chem. Mater.* **2001**, *13*, 2567−2573.
(37) Passuello, T.; Piccinelli, F.; Pedroni, M.; Mangiarini, F.; Vetrone, F.; Bettinelli, M.; Speghini, A. *Opt. Mater.* **2011**, *33*, 1500−1505.
(38) Wu, J. H.; Wang, J. L.; Lin, J. M.; Xiao, Y. M.; Yue, G. T.; Huang, M. L.; Lan, Z.; Huang, Y. F.; Fan, L. Q.; Yin, S.; Sato, T. *Sci. Rep.* **2013**, DOI: 10.1038/ srep02058.
(39) Ko, K.; Lee, Y.; Jung, Y. *J. Colloid Interface Sci.* **2005**, *283*, 482−487.
(40) Murakoshi, K.; Kano, G.; Wada, Y.; Yanagida, S.; Miyazaki, H.; Matsumoto, M.; Murasawa, S. *J. Electroanal. Chem.* **1995**, *396*, 27−34.
(41) Rothenberger, G.; Fitzmaurice, D.; Grätzel, M. *J. Phys. Chem.* **1992**, *96*, 5983−5986.
(42) Cardon, F.; Gomes, W. P. *J. Phys. D: Appl. Phys.* **1978**, *11*, L63−L67.
(43) Grätzel, M. *Nature* **2001**, *414*, 338−344.
(44) Zhao, J. X.; Lu, X. H.; Zheng, Y. Z.; Bi, S. Q.; Tao, X.; Chen, J. F.; Zhou, W. L. *Electrochem. Commun.* **2013**, *32*, 14−17.
(45) Zhang, Y.; Zhang, W.; Xie, T. F.; Wang, D. J.; Song, X. M. *Mater. Res. Bull.* **2013**, *48*, 3242−3246.
(46) Guo, F. A.; Li, G. Q.; Zhang, W. F. *Int. J. Photoenergy* **2010**, DOI: 10.1155/2010/105878.
(47) Miao, X. H.; Pan, K.; Liao, Y. P.; Zhou, W.; Pan, Q. Q.; Tian, G. H.; Wang, G. F. *J. Mater. Chem. A* **2013**, *1*, 9853−9861.
(48) Wang, Q.; Moser, J. E.; Grätzel, M. *J. Phys. Chem. B* **2005**, *109*, 14945−14953.
(49) Shang, G. L.; Wu, J. H.; Tang, S.; Liu, L.; Zhang, X. P. *J. Phys. Chem. C* **2013**, *117*, 4345−4350.
(50) Balaji, S.; Mandal, A. K.; Annapurna, K. *Opt. Mater.* **2013**, *34*, 1930−1934.